Available online at www.sciencedirect.com
SCIENCE DIRECT®
Journal of Nuclear Materials 329–333 (2004) 1466–1470
journal of nuclear materials
www.elsevier.com/locate/jnucmat

Relation between macroscopic length change and the crystal structure in heavily neutron-irradiated ceramics

Masafumi Akiyoshi [a,*], Naoaki Akasaka [a], Yoshiaki Tachi [a], Toyohiko Yano [b]

[a] *MMS, O-arai Engineering Center, Japan Nuclear Cycle Development Institute, 4002 Narita-cho, O-arai-machi, Higashi-Ibaraki-gun, Ibaraki-ken 311-1393, Japan*
[b] *Tokyo Institute of Technology, 2-12-1 O-okayama, Meguro-ku, Tokyo 152-8550, Japan*

Abstract

Macroscopic length changes of heavily neutron-irradiated α-Al_2O_3, AlN, β-Si_3N_4 and β-SiC were measured and analyzed, and the results were elucidated by considering the crystal structure of each material. These specimens were irradiated under the same conditions (775–1039 K, $2.8–7.3\times10^{26}$ n/m^2) in the experimental fast reactor JOYO. Alpha-Al_2O_3 and AlN showed large length change compared with that of β-Si_3N_4 and β-SiC. In α-Al_2O_3 and AlN, interstitial dislocation loops are inserted mainly into the (0 0 0 1) plane, and they do not interfere with each other. Therefore, new loops are induced without any restriction and anisotropic lattice stretching induces intergranular cracking. On the other hand, interstitial dislocation loops are inserted into $\{1\,0\,\bar{1}\,0\}$ or $\{1\,1\,\bar{2}\,0\}$ planes in β-Si_3N_4 and {1 1 1} planes in β-SiC. These planes of forms have several symmetrical planes, and dislocation loops on them interfere with each other to form nano-partitions. So, growth and nucleation of loops are limited, and induced Frenkel pairs only recombine with each other.

1. Introduction

Ceramic materials are expected to be used in many nuclear applications such as inert materials for nuclear transmutation, fuel coatings in fission reactors, and blanket, insulators and radio-frequency power injection windows in fusion reactors [1–6]. In particular, very high radiation stability qualifies β-SiC and β-Si_3N_4 to be some of the most encouraging ceramic materials for thermonuclear fusion reactors where they would be exposed to high fluence of 14 MeV fusion neutrons at temperatures up to 1300 K.

In these environments, materials undergo severe property changes such as swelling, degradation of thermal diffusivity, mechanical strength and so on. High-energy neutron-irradiation induces several types of crystalline defects in ceramic materials. At first, knock-on cascades leave Frenkel pairs and other point-like defects, and they are immobile at lower temperatures, so the density of point defects is determined by the recombination radius. When materials are irradiated at higher temperatures (around 600 K), mobility of point defects increases and they should aggregate and grow to form dislocation loops or voids. These dislocation loops are induced mainly in the closest packed plane, and sometimes they give anisotropic swelling in each grain depending on a crystal structure of each material. Finally, large anisotropic swelling in each grain induces intergranular cracks. In addition, neutron irradiation transmutes some nuclide to gas atoms that causes to induce bubbles. Macroscopic length change is influenced by the amount and type of all these defects.

Ceramic materials have many different crystallographic structures, bonding type, bonding energy and elements with each material, even the physical properties vary with the sintering method or sintering additives for

* Corresponding author. Tel.: +81-29 267 4141x5539; fax: +81-29 266 3713.
E-mail address: akiyoshi.masafumi@jnc.go.jp (M. Akiyoshi).

0022-3115/$ - see front matter © 2004 Elsevier B.V. All rights reserved.
doi:10.1016/j.jnucmat.2004.04.251

the same material. In this paper, measurements of macroscopic length changes were carried out for heavily-neutron-irradiated α-Al_2O_3, AlN, β-Si_3N_4 and β-SiC they were irradiated under the same conditions. Some of them were reported in our previous papers [7,8], but additional data on swelling for each specimen are presented, and the data are compared for these four kinds of ceramics. The differences are arise from many factors given above, nevertheless in this paper, we discuss the swelling behavior from the viewpoint of crystal structure for each material. Transmission electron microscopy (TEM) observations have shown that the distribution of these defects directly, and careful high resolution electron microscopy (HREM) observations enable us to obtain crystallographic information on these defects.

2. Experimental procedure

The α-Al_2O_3, AlN, β-Si_3N_4 and β-SiC specimens were manufactured by Nippon Steel and Tokukama. Alpha-Al_2O_3 and AlN were sintered by a pressureless method and β-Si_3N_4 and β-SiC by a hot-press method. All specimens were sintered to almost full density; their details are given in Table 1. Specimen dimensions were $1.2\times1.2\times15.5$ mm for α-Al_2O_3 and β-Si_3N_4, and $1.2\times1.2\times14.5$ mm for AlN and β-SiC.

Neutron-irradiation was performed in the Japanese experimental fast reactor JOYO, using the irradiation rigs CMIR-4 and CMIR-5 to fluences of $2.8–7.3\times10^{26}$ n/m^2 at 775–1039 K. The irradiation conditions are listed in Table 2 with the results of macroscopic length measurement. The irradiation temperatures were estimated from TED temperature monitors. On the other hand, in our previous studies [7–9], irradiation temperature was estimated by calculations, which led to a small difference between them and the present study. The measurement of the macroscopic length change was performed by conventional flat-type micrometer at room temperature.

3. Results and discussion

Table 2 shows the macroscopic length change (linear swelling) after neutron-irradiation for α-Al_2O_3, AlN, β-Si_3N_4 and β-SiC. The results showed obvious differences between Al base materials (α-Al_2O_3 and AlN) and Si base materials (β-Si_3N_4 and β-SiC), i.e. α-Al_2O_3 and

Table 1
Details of ceramic specimens studied

Material	α-Al_2O_3	AlN	β-Si_3N_4	β-SiC
Manufacturer	Nippon Steel	Tokuyama	Nippon Steel	Nippon Steel
Type	NSAR	SuperShapal	NS101	SiC
Raw material	α-Al_2O_3 100 wt%	AlN (unknown)	β-Si_3N_4 > 88 wt% Y_2O_3 < 10 wt% $ZrSi_2$ < 2 wt%	β-SiC > 99 wt% Al_2O_3 < 1 wt%
Sintering method	Pressureless	Pressureless	Hot press	Hot press
Relative density	99.5%	~99.9%	100%	99.7%
Crystal system	Hexagonal	Hexagonal	Hexagonal	Cubic
Space group	D^6_{3D}–$R\bar{3}c$	$P6_3mc$	$P6_3/m$	$F\bar{4}3m$
Lattice constant				
$a = b$ (nm)	0.4758	0.3114	0.7604	0.4359
c (nm)	1.2991	0.49792	0.290751	$= a$
Dislocation loops	(0 0 0 1)	(0 0 0 1)	$\{1\,0\,\bar{1}\,0\}$, $\{1\,1\,\bar{2}\,0\}$	{1 1 1}
Burgers vector	$\frac{1}{3}\langle1\,0\,\bar{1}\,1\rangle$	$\frac{1}{2}$[0 0 0 1]	$\frac{1}{18}\langle\bar{2}\,4\,\bar{2}\,9\rangle$, $\frac{1}{18}\langle22\bar{4}9\rangle$	$\frac{1}{3}\langle1\,1\,1\rangle$

Table 2
Irradiation conditions of specimens and changes in macroscopic length

ID	Dose (n/m^2)	Temperature (K)	Macroscopic length change (%)			
			α-Al_2O_3	AlN	β-Si_3N_4	β-SiC
T61	2.8×10^{26}	775	1.11	2.00	0.19	0.42
T63	3.9×10^{26}	864	1.77	1.92	0.36	0.40
T64	7.3×10^{26}	835	2.59	2.24	0.40	0.30
T65	4.2×10^{26}	1004	2.26	2.00	0.23	0.45
T67	3.7×10^{26}	1011	1.96	1.78	0.16	0.35
T68	6.9×10^{26}	1039	2.30	2.30	0.30	0.54

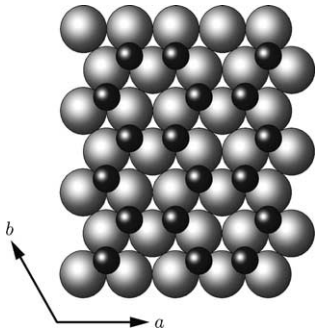

Fig. 1. Crystal structure model of α-Al_2O_3 projected onto the (0 0 0 1) plane. Large, gray circles represent oxygen ions, and small, black circles represent aluminum ions. Aluminum cations occupy two-thirds of the octahedral interstices in the hexagonal close-packed structure of oxygen anions.

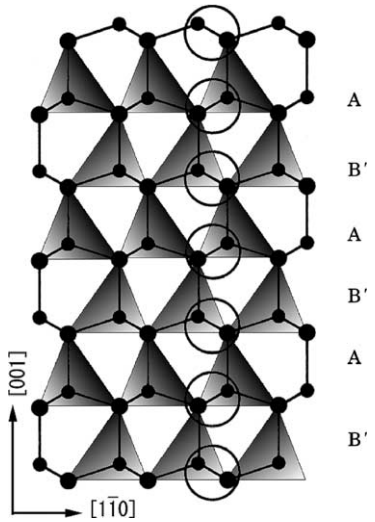

Fig. 2. Crystal structure of AlN projected onto the (1 1 $\bar{2}$ 0) plane. AlN_4 tetrahedra are arranged alternately along the [0 0 1] direction. Small dots located at the center of each tetrahedron represent Al atoms, and large dots located at each corner of the tetrahedron represent N atoms.

AlN showed a large length change of 1.11–2.59% while β-Si_3N_4 and β-SiC showed a small one of 0.16–0.54%. In particular, β-Si_3N_4 had a smaller length change than β-SiC except for the T64 specimen.

The results in this study were explained from the viewpoint of crystal structure. Figs. 1–5 show a crystal structure model for each material.

In Fig. 1, a crystal structure model of α-Al_2O_3 is projected onto the (0 0 0 1) plane. Aluminum cations occupy two-thirds of the octahedral interstices in the hexagonal close-packed structure of oxygen anions. The close-packing plane is the (0 0 0 1) plane and it was reported that interstitial dislocation loops were

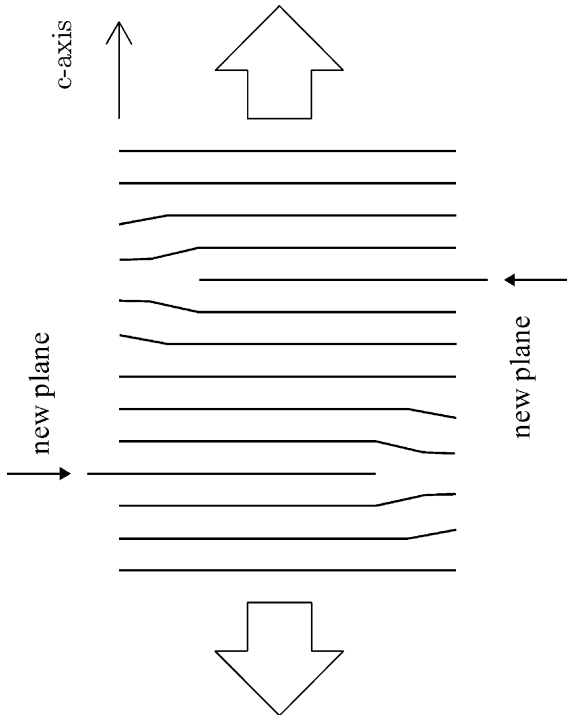

Fig. 3. Structure image model of piled up dislocation loops nucleated on the (0 0 0 1) plane.

predominantly induced into the (0 0 0 1) plane having a Burgers vector $\boldsymbol{b} = \frac{1}{3}[1\,0\,\bar{1}\,1]$ [10,11].

In Fig. 2, crystal structure of AlN is projected onto the (1 1 $\bar{2}$ 0) plane. AlN_4 tetrahedra are arranged alternately along the [0 0 0 1] direction. The close-packing plane is the (0 0 0 1) plane and it was reported that interstitial dislocation loops were induced into the (0 0 0 1) plane having a Burgers vector $\boldsymbol{b} = \frac{1}{2}$ [0 0 0 1] [12,13].

Interstitial dislocation loops in both α-Al_2O_3 and AlN were formed on the hexagonal basal plane (0 0 0 1), and these loops were piled up in parallel (a schematic model is shown in Fig. 3). Therefore, they did not restrain induction of new loops on this plane or growth and coalescence with loops on the same plane, and it caused unrestrained elongation in the *c*-axis. Finally, this anisotropic elongation led to intergranular cracking.

On the other hand, β-Si_3N_4 and β-SiC have different close-packing planes. In Fig. 4, a simplified crystal structure model of β-Si_3N_4 is projected onto the (0 0 0 1) plane. All atom sites are approximated as multiples of $\frac{1}{12}$ of the unit cell length of the *a*-axis and SiN_4 tetrahedra are approximated as equilateral triangles in this projection [14]. The structure contains six-membered, corner-shared SiN_4 tetrahedral rings, with relatively large open channels at their centers that penetrate the crystal along the *c*-axis. The close-packing plane is the {1 0 $\bar{1}$ 0}

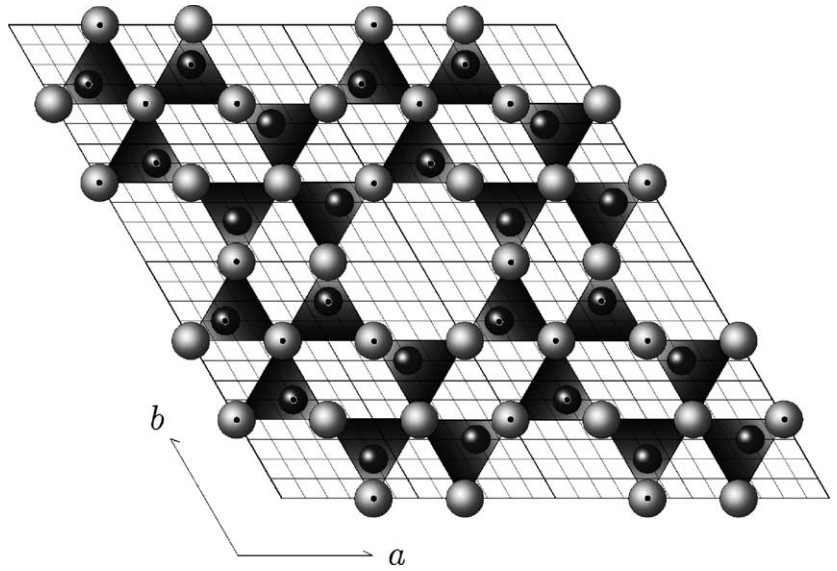

Fig. 4. Simplified model of β-Si_3N_4 projected onto the (0 0 0 1) plane. All atom sites are approximated as multiples of $\frac{1}{12}$ of the unit cell length of the *a*-axis. SiN_4 tetrahedra are approximated as equilateral triangles in this projection. Atoms on the layer at $z = \frac{1}{4}$ are shown with a small black dot at their center and atoms at $z = \frac{3}{4}$ are shown without a dot. Large grey circles represent N atoms, and medium black circles represent Si atoms. The base edges of tetrahedra, which connect two N atoms with the same *z* parameter, are shown with heavier gradation.

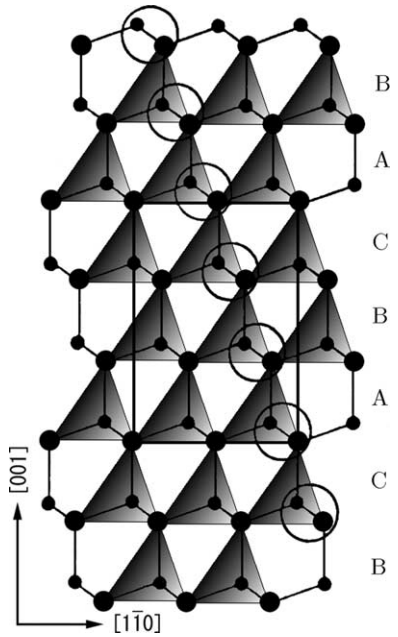

Fig. 5. Crystal structure of β-SiC projected onto the (1 1 0) plane. SiC_4 tetrahedra are arranged in the same orientation along the [1 1 1] direction. Small dots located at the center of tetrahedron represent Si atoms, and large dots located at each corner of tetrahedron represent C atoms.

prismatic planes, and we clarified that interstitial dislocation loops were induced into those $\{1\,0\,\bar{1}\,0\}$ planes having a Burgers vector $\boldsymbol{b} \simeq \frac{1}{18}\langle\bar{2}\,4\,\bar{2}\,9\rangle(\frac{1}{6}\langle 0\,2\,3\rangle)$, corresponding to an extra layer of SiN_4 tetrahedra inserted into the $\{1\,0\,\bar{1}\,0\}$ planes [14]. It is noted that the $\{1\,0\,\bar{1}\,0\}$ family of habit planes have three crystallographically equivalent planes in the hexagonal lattice, so equivalent defects can be induced in these three planes, which are rotated 60° or 120° from the $\{1\,0\,0\}$ plane. In addition, another type of planar defect was induced into the $\{1\,1\,\bar{2}\,0\}$ planes having a Burgers vector $\boldsymbol{b} \simeq \frac{1}{18}\langle 2\,2\,\bar{4}\,9\rangle(\frac{1}{6}\langle 2\,2\,3\rangle)$, and the $\{1\,1\,\bar{2}\,0\}$ planes of a form also has three equivalent planes [15]. Furthermore, these two types of defects have a connecting structure in a particular arrangement, but never cross each other [16].

In Fig. 5, crystal structure of β-SiC is projected onto the (1 1 0) plane. SiC_4 tetrahedra are arranged in the same orientation along the [1 1 1] direction. The close-packing plane is the [1 1 1] planes of a form and it was reported that interstitial dislocation loops were induced into those $\{1\,1\,1\}$ planes having a Burgers vector $\boldsymbol{b} = \frac{1}{3}\langle 1\,1\,1\rangle$ [13,17]. The $\{1\,1\,1\}$ planes have four crystallographically equivalent planes in the cubic lattice, corresponding to each face of a SiC_4 tetrahedron.

These dislocation loops in β-Si_3N_4 and β-SiC were not induced into only parallel planes and their structure does not allow intersection in the same plane, so they restricted growth of loops or induction of new loops. Therefore, in these saturated crystals, dislocation loops could not act as sinks of interstitial atoms any more, and they stayed as a nanometer-sized partition. Consequently, additional interstitial atoms and vacancies

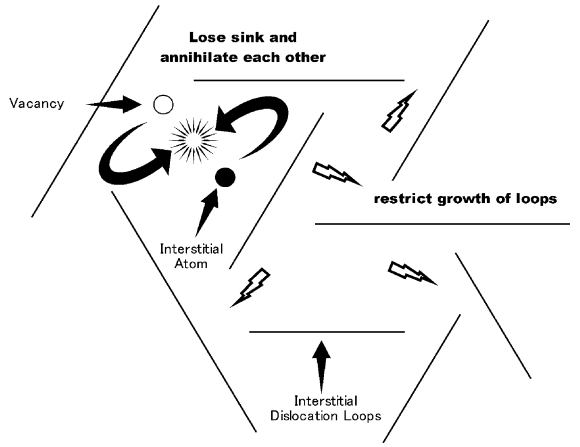

Fig. 6. Schematic model of nano-partitions (dislocation loops which restrict each others growth).

would only annihilate each other. We named this dislocation structure 'nano-partition' (a schematic model was shown in Fig. 6). This nano-partition structure restricted the swelling. Of cause, many factor affect to swelling, such as void formation, but the plane where interstitial dislocation loops are induced gives quite important information to forecast the swelling behavior.

4. Conclusion

Macroscopic length change measurements were performed for neutron-irradiated α-Al_2O_3, AlN, β-Si_3N_4 and β-SiC. It was clarified that α-Al_2O_3 and AlN had a large length change of 1.11–2.59% while β-Si_3N_4 and β-SiC had small one of 0.16–0.54%. This difference was discussed from the viewpoint of crystal structure. In the case of α-Al_2O_3 and AlN, the close-packing plane is the (0 0 0 1) plane, and interstitial dislocation loops were piled up in parallel without any restriction on inducing a new loop, or growing and coalescing with loops on the same plane, so unrestrained elongation in the *c*-axis was caused. On the other hand, for β-Si_3N_4 and β-SiC, close-packing planes are $\{1\,0\bar{1}\,0\}$ and $\{1\,1\,1\}$ planes of forms, respectively, and interstitial dislocation loops were induced into $\{1\,0\bar{1}\,0\}$ and $\{1\,1\bar{2}\,0\}$ planes in β-Si_3N_4 and $\{1\,1\,1\}$ planes in β-SiC. These planes cross each other, but the loop structures could not intersect, so they restricted growth of loops or nucleation of new loops. In this nano-partition structure, additional interstitial atoms and vacancies only annihilated each other, and it restricted the swelling.

References

[1] G.F. Dell, A.N. Goland, J. Nucl. Mater. 102 (1981) 246.
[2] F.W. Clinard Jr., G.F. Hurley, R.W. Klaffky, Res. Mech. 8 (1983) 207.
[3] G.P. Pells, J. Nucl. Mater. 122&123 (1984) 1338.
[4] F.W. Clinard Jr., G.F. Hurley, L.W. Hobbs, D.L. Rohv, R.A. Youngman, J. Nucl. Mater. 122&123 (1984) 1386.
[5] G.R. Hopkins, R.J. Price, Nucl. Eng. Des./Fus. 2 (1985) 111.
[6] C. Kinoshita, S. Zinkle, J. Nucl. Mater. 233–237 (1996) 100.
[7] T. Yano, K. Ichikawa, M. Akiyoshi, Y. Tachi, J. Nucl. Mater. 283–287 (2000) 947.
[8] T. Yano, M. Akiyoshi, K. Ichikawa, Y. Tachi, Y. Iseki, J. Nucl. Mater. 289 (2001) 102.
[9] M. Akiyoshi, K. Ichikawa, T. Donomae, T. Yano, J. Nucl. Mater. 307–311 (2002) 1305.
[10] R.A. Youngman, T.E. Mitchell, F.W. Clinard Jr., G.F. Hurley, J. Mater. Res. 6 (1991) 2178.
[11] C. Kinoshita, K. Fukumoto, K. Fukuda, F.A. Garner, G.W. Hollenberg, J. Nucl. Mater. 219 (1995) 143.
[12] T. Yano, T. Iseki, Philos. Mag. Lett. 62 (1990) 82.
[13] T. Yano, J. Ceram. Soc. Jpn. 111 (2003) 155.
[14] M. Akiyoshi, T. Yano, M. Jenkins, Philos. Mag. A 81 (2001) 683.
[15] M. Akiyoshi, T. Yano, M. Jenkins, Philos. Mag. Let. 81 (2001) 251.
[16] M. Akiyoshi, T. Yano, J. Electron Microsc. 52 (2003) 267.
[17] T. Yano, T. Iseki, Philos. Mag. A 62 (1990) 421.